Paradigm Academic Press
Innovation in Science and Technology
ISSN 2788-7030
MAY. 2023 VOL.2, NO.3

Study on the Influence of Car Meeting on Disturbance Transfer Characteristics of Platoon-Driving

Hongtao Tang[1], Xiang Zhang[1] & Nenghui Zhou[2]

[1] College of Mechanical Engineering, Tianjin University of Science & Technology, Tianjin 300222, China

[2] Tianjin Yidingfeng Power Technology Co., Ltd, Tianjin 300380, China

Correspondence: Nenghui Zhou, Tianjin Yidingfeng Power Technology Co., Ltd, Tianjin 300380, China.

doi:10.56397/IST.2023.05.07

Abstract

The overlapping grid method is a novel region segmentation and grid combination strategy. Based on this method, the aerodynamic characteristics of lineup vehicles in meeting conditions are simulated in this paper. Firstly, the data obtained from the single-vehicle simulation is compared with the wind tunnel test data, and the error value is relatively small, which verifies the validity of the overlapping grid method. After that, simulation was carried out to analyze the changes of flow field around the cars in formation, and the differences between the front and rear cars in formation were summarized. Finally, the vehicle pressure field, velocity field, aerodynamic coefficient and torque coefficient were statistically analyzed, and the influence of the car meeting on the aerodynamic characteristics of the queue was studied.

Keywords: platoon-driving, overlapping grids, car meeting, aerodynamic coefficient

1. Introduction

Platoon-driving is when two or more vehicles keep a certain distance behind each other while driving, thereby effectively utilizing aerodynamic characteristics and achieving energy saving and emission reduction. (Guanghan Peng, Shuhong Yang, Dongxue Xia & Xiaoqin Li, 2019) Nowadays, with the development of digital mapping, sensing, V2V communication and other technologies, platooning has attracted more and more attention.

In recent years, many scholars at home and abroad have done wind tunnel tests and simulation on the driving condition of cars in formation. For example, Charles-Henri Bruneau et al. (Charles-Henri Bruneau, Khodor Khadra & Iraj Mortazavi, 2017) used a simplified model to simulate the flow field characteristics of buses in formation. Jiang Tao et al. (Jiang Tao, Shi Yan, Xu Peipei, Wang Min & Li Yao, 2022) analyzed and compared the simulation data of two-car procession and three-car procession; Li Mingda et al. (Li Mingda, Wei Hailin, Men Yuzhuo & Bao Cuizhu, 2018) studied the fuel economy of tank cars in formation; Francis H. Robertson et al. (Francis H. Robertson, Frederick Bourriez, Mingzhe He, David Soper, Chris Baker, Hassan Hemida & Mark Sterling, 2019) carried out transient tests on eight truck models; Xiao Tian Zhang et al. (Xiao-Tian Zhang, Francis H. Robertson, David Soper, Hassan Hemida & Shi-Di Huang, 2021) studied the variation of aerodynamic resistance of long trucks queuing through a tunnel, and the conclusions of these simulation tests all show the aerodynamic advantages of cars queuing up to a certain extent. However, most of these studies focus on large vehicles such as buses and trucks, which may be because the drag reduction effect of large vehicles is more significant when they drive in formation. However, it is also necessary to simulate cars in procession. Therefore, this paper will choose the representative MIRA car model to conduct simulation research under the working condition of cars in procession.

At present, the simulation research methods of transient aerodynamic characteristics of vehicles can be roughly

divided into three categories: dynamic grid, sliding grid and overlapping grid. For example, Feng Yibin et al. (Feng Yibin & Guo Xuexun, 2008), Gao Long et al. (Gao Long & Zhou Haichao, 2012), Tang Hongtao et al. (Tang Hongtao, Miao Xiuqi, Chen Guanghou & Dong Linyuan, 2018), used dynamic grid technology to study the aerodynamic characteristics of vehicles under overtaking and meeting conditions. Gu Zhengqi et al. (Zhang Yingchao, Li Jie, Li Yuhu, Hu Xingjun & Fu Limin, 2008) and Zhang Yingchao et al. (Gu Zhengqi, Yang Binhui, Gong Xu, Sun Lu & Yuan Zhiqun, 2010) studied the aerodynamic characteristics of cars during parking by using the sliding grid method. Wang Jingyu et al. (Wang Jingyu, Yu Xutao, Hui Zheng & Hu Xingjun, 2017) used the overlapping grid method to simulate the aerodynamic characteristics of cars in curves.

Because of the novelty of the overlapping grid method, the application of this method in the field of automotive CFD is relatively few. Therefore, this paper will use this method to simulate rectilinear driving conditions of a single vehicle, and compare the results with the wind tunnel test data to verify its effectiveness. Then, the simulation calculation will be carried out for the platoons under the driving conditions of vehicles, to observe the changes in the flow field and summarize the aerodynamic changes.

2. Numerical Simulation

2.1 Introduction to Overlapping Grids

overlapping grids, also known as overset grids, are composed of background grids and component grids. They have overlapping areas spatially by using the “burrow” technology. Data can be transferred between overlapping areas or interfaces through the establishment of an embedding relationship. In this way, the flow field information in the whole computing domain can be obtained.

“Hole digging” refers to the processing of different grid units in the process of grid assembly, which are divided into cavity units, computing units and interpolation units. The cavity units do not participate in the simulation calculation of the flow field, and this process is called “hole digging”. The establishment of the embedding relation is actually the process of establishing the interpolation relation in the overlapping area and the junction. (Li Peng, Gao Zhenxun & Jiang Chongwen, 2014)

At present, moving grid, sliding grid and overlapping grid are the main methods to study the transient aerodynamic characteristics of vehicles. The sliding grid method can only simulate simple reciprocating and rotating motion conditions, so it is often used in the simulation of linear vehicle driving. The dynamic grid method can be applied to complex and complicated vehicle motion conditions, but the premise of its use is generally to make quite high quality grids, and in the grid reconstruction also face the problem of distortion and deformation, and occupy a lot of computing resources and time, so it is difficult to use under limited conditions. The emergence of the overlapping grid method makes these problems be dealt with effectively. The most outstanding advantage of the overlapping grid method is that it can not only generate the most appropriate grid in different calculation areas, simplify the difficulty of grid division in practical engineering problems and ensure the quality of the grid, but also load the UDF in the dynamic grid to simulate and calculate the complex and complicated vehicle working conditions. It can save a lot of computing resources and time. However, it should be noted that in order to ensure the accuracy of interpolation calculation, the mesh size of overlapping area should be kept as consistent as possible.

2.2 Model Size and Calculation Domain Determination

Tab.1 shows the basic size of the MIRA vehicle model. This model is selected because there are more wind tunnel test and outflow field simulation data of this model in previous studies, which facilitates the accuracy verification of the simulation method adopted in this paper. Figure 1 shows the geometric model of MIRA built using ANSYS SpaceClaim software. The area of the model’s positive projection is 1.856m^2.

Table 1. Basic dimensions of MIRA car model

Serial number	Name	Size (mm)
1	Total length	4165
2	Total width	1625
3	Total height	1421
4	Hood length	1055
5	Trunk length	750
6	Ceiling height	508
7	Canopy width	1420

8	Lower body height	708
9	Ground clearance	205
10	Tire radius	705

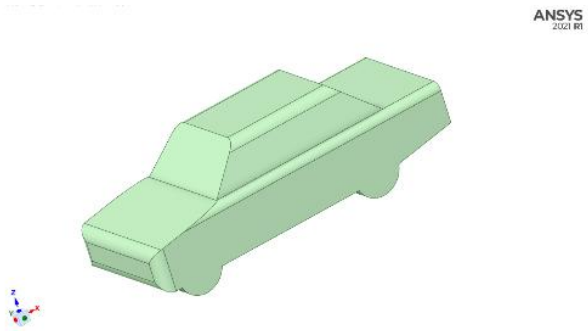

Figure 1. MIRA geometric model

The simulation in this paper includes three working conditions: single vehicle driving, platooning-driving, and platooning-driving of car meeting condition. In order to ensure the validity of data comparison results, the same setting conditions are adopted in the calculation domain. Taking the queue car meeting condition in Figure 2 as an example, the length of the calculation domain is 16L=74.97m, and the distance between the car tail and the boundary of the calculation domain at the initial position is 4L=16.66m. The width of the computing domain is 14m, and the distance between the side of the car and the computing domain is 3W=4.875m; The height of the computing domain is 4H=5.684m, where the three small rectangular blocks surrounding the car are the parts area generated by Boolean operation with the car geometry.

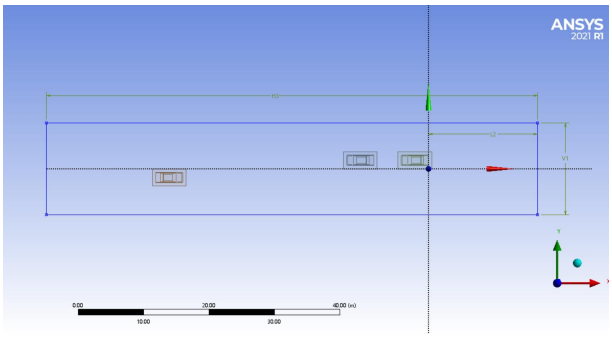

Figure 2. Computing domain model

2.3 Meshing

Before grid meshing, it is necessary to cut the background grid area. Since the car is in a straight line driving state in this case, it is only necessary to encrypt the grid of the car driving area, so that the mesh size of the encrypted area is consistent with that of the component grid, so as to be more accurate in interpolation calculation. The grid division situation is shown in Figure 3. In the background grid, the size of both the vehicle driving area and the component grid is set at 0.1m, and boundary layer encryption is carried out on the body surface, the number of layers is 5, and the transition ratio is 1.2. The boundary layer grid division is shown in Figure 4.

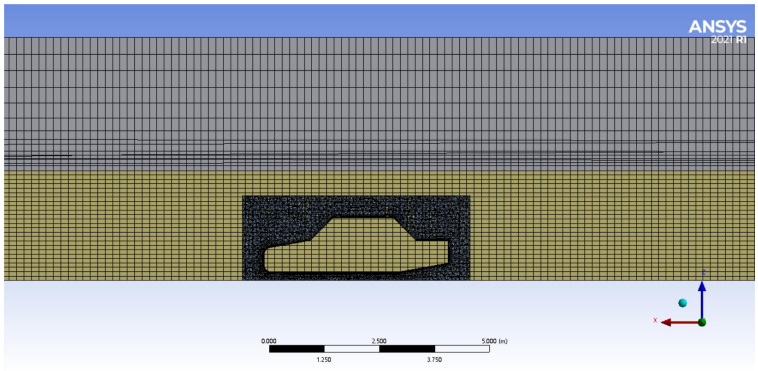

Figure 3. Grid meshing

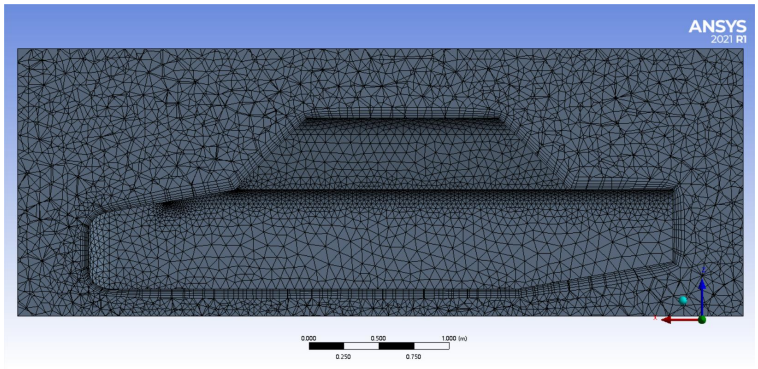

Figure 4. Boundary layer grid

2.4 Scheme Design and Solution Setup

As shown in Figure 5, the vehicles in the queue are denoted as Car-A and Car-B, in which Car-B follows Car-A, and the vehicles coming in the opposite direction are denoted as Car-C. The speed V of each vehicle is set at 25m/s and keeps constant. In general, air is considered an incompressible fluid when the airflow velocity is less than one-third of the speed of sound. In this paper, the vehicle speed is far less than this value index, so the surrounding air is considered as an incompressible fluid when the vehicle is driving.

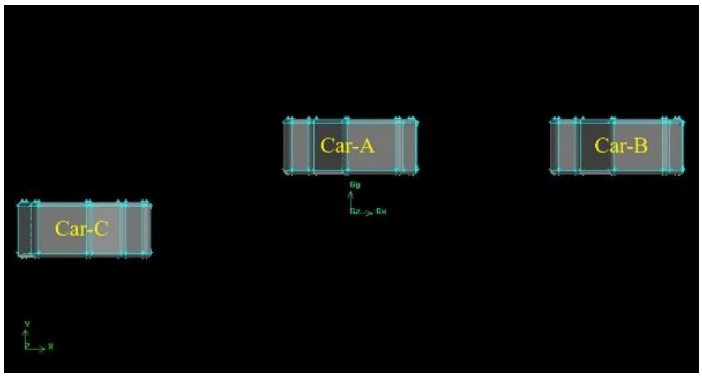

Figure 5. Car number

In order to better reflect the influence of cars meeting on the aerodynamic characteristics of platooning-driving, the overall calculation domain was set as the pressure outlet on both the left and right sides to simulate the ideal environment under open and windless conditions. A transient solver was used and Realizable k-epsilon turbulence model was selected, as shown in Figure 6. Most Y^+ values of the car body were concentrated between 30 and 300, and a large number of air backflow and vortices appeared around the car body due to the influence of car geometry, procession driving and meeting conditions. Therefore, it is necessary to add Non-Equilibrium Wall Functions, which can more truly reflect the air flow situation outside the car. In order to make the

calculation more accurate and conducive to data collection, a small Time Step is set, Time Step Size=0.00104125s, time step number is 1660, and the flow field change within 1.66s is calculated. Within the first 50 steps, more iterations are set to ensure that the air in the flow field is fully flowing after the first 50 steps of calculation. After that, automatic saving and data monitoring Settings are carried out, and simulation results and data are saved every 10 steps for subsequent sorting and analysis.

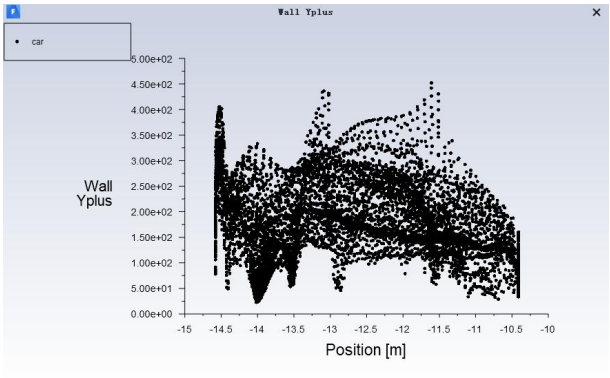

Figure 6. Y^+ value of vehicle

3. Analysis of Single-Vehicle Simulation

The previous CFD simulation idea of single-vehicle outflow field is similar to wind tunnel test. The vehicle model is set as a static rigid body, the speed inlet is set at the boundary of the calculation domain, and a certain air velocity is given to simulate the movement of surrounding air when the vehicle is running. In the single-vehicle simulation in this paper, the component grid containing the MIRA model is set as a moving rigid body, the speed is 25m/s, and the boundary conditions are set as the default pressure inlet and pressure outlet by using the overlapping grid method. In this way, the accuracy of the overlapping grid method can be judged by comparing the simulation result data with the wind tunnel test data.

3.1 Analysis of Contours of Pressure

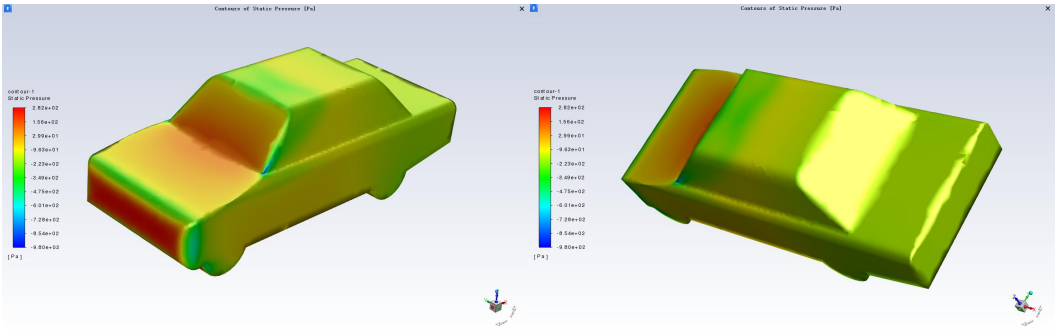

Figure 7. Contours of pressure of MIRA surface

Figure 7 shows the contours of pressure of the of MIRA surface during driving. The pressure difference between the front and rear of the car is significant, which is the main source of the air resistance of the car. The maximum pressure value is 282Pa, which is located in the central grid of the car. Strong eddy current will be generated. At the junction of the car net and bonnet, and at the junction of the front windshield and ceiling, most of the air flow is no longer attached to the body surface and separated, resulting in reduced pressure at these positions. After a certain distance, the air flow will re-attach to the car surface, making the pressure on the bonnet and ceiling slowly increase along the body surface, which is in line with the actual situation.

3.2 Analysis of Aerodynamic Coefficient

During calculation, only when the time step number reaches more than 50 times can the air in the flow field fully flow, and the aerodynamic characteristics of the vehicle enter a relatively stable state. Figure 8 captures the aerodynamic coefficient data of the vehicle between 260 and 280 time steps. As is known to all, the biggest

source of vehicle driving resistance is the pressure difference between the front and rear of the vehicle body. As shown in Figure 8(a), the body resistance coefficient changes constantly between 0.330 and 0.344, and the fluctuation range is small, because the pressure difference between the front and rear will change slightly with the change of the vortex energy of the surrounding air in the process of vehicle driving. Large lateral force and yaw moment will affect the vehicle's driving stability. As shown in Figure 8(b), the lateral force coefficient of the vehicle body is almost 0 in single-vehicle driving condition, and the fluctuation range is between -0.002 and 0.002. The lateral force coefficient formula is used for conversion, and it can be seen that the lateral force of the vehicle body is between -10N and 10N. This has little impact on the vehicle's driving stability; As 35%~40% of the air acting on the vehicle body flows from above and 10%~15% from below during the driving process, and the downward pressure is generated in the direction perpendicular to the road due to the influence of the geometry of the vehicle body, making the lift coefficient of the vehicle body negative, as shown in Figure 8(c).

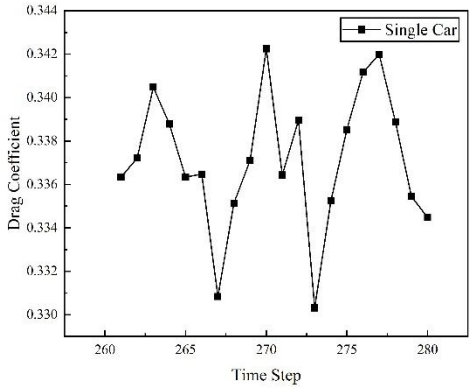

(a) Single-vehicle resistance coefficient

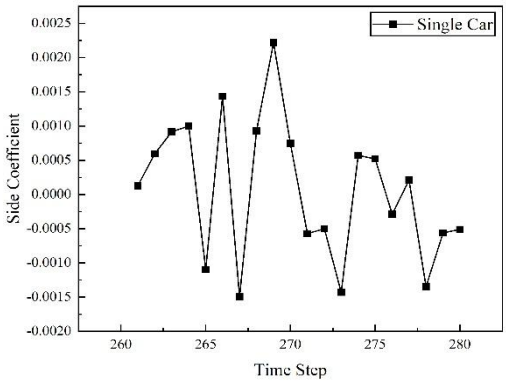

(b) Single-vehicle lateral force coefficient

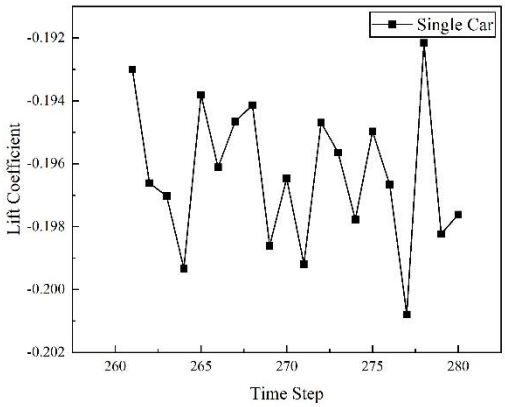

(c) Lift coefficient of the single vehicle

Figure 8. Aerodynamic coefficient of single bike

After sorting out the transient simulation results of MIRA single-vehicle model, the average drag coefficient is 0.3371. The University of Stuttgart and Hunan University have carried out a series of wind tunnel tests on the MIRA vehicle model, and the wind resistance coefficients obtained from the tests are 0.3204 and 0.3225, respectively. The simulation data is compared with the wind tunnel test data (Chen Jianhong, 2015; Zhang Yingchao, Cao Huinan & Zhu Hui, 2019; Wang Shi, 2011), as shown in Tab.2. There is a certain error between the simulation data and the wind tunnel test data, but the error value is controlled within a small range, no more than 7%. On the one hand, the error may be due to the difference between the geometric model used in the simulation experiment and the solid model in the wind tunnel test; on the other hand, it may be because the conditions used in the simulation calculation are more idealized than those in the wind tunnel.

Table 2. Air drag coefficient of MIRA model

Data sources	Drag coefficient	Relative error

Simulation simulation	0.3371	/
Wind tunnel test of Hunan University	0.3204	5.2%
Wind tunnel test of Stuttgart University	0.3225	4.5%

In general, the data obtained by using the overlapping grid method for transient simulation of vehicles is more accurate, so the numerical simulation method adopted in this paper is effective and reliable. Subsequently, the method will be used to simulate the platoon-driving conditions.

4. Analysis of the Simulation of Platoon-Driving

The spacing between the front and back of the cars in formation was set as 1 Car length, and the two cars were traveling at the same speed, both of which were 25m/s. The front Car was CAR-A and the rear car was Car-B.

4.1 Chart of Contours and Streamlines

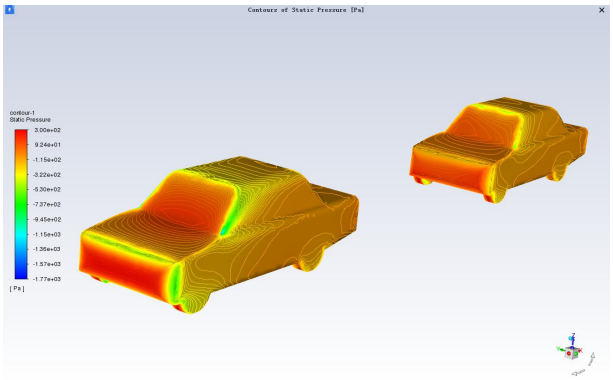

Figure 9. Pressure cloud diagram of cars in formation

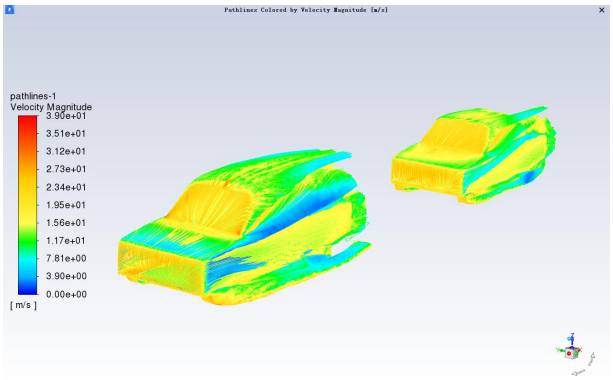

Figure 10. Flow diagram of cars in formation

Figure 9 shows the pressure cloud image of cars in formation at a certain time. Select the option contour lines to facilitate the observation of pressure changes on the body surface. The air pressure on the front of Car-A is significantly higher than that on the front of Car-B, and the pressure gradient on the body surface changes more significantly, and the pressure contour lines are arranged more densely, which is the main reason that the air resistance of Car-A is greater than that of Car-B. In addition, at the junction of different geometric surfaces on the front of the car, even if the geometric shape is filleted, there is still an obvious air separation phenomenon, as shown in Figure 10, which will lead to obvious negative pressure at these junction locations. Due to the separation and reattachment of air flow, Car-B is affected by the disturbance of air flow through the Car-A body, which weakens the air separation effect and makes the negative pressure strength at the junction of the front Car-A body surface greater than that of Car-B. In the front windshield of CAR-A, the high-pressure area is located near the central axis of the Car, and in the front windshield of CAR-B, the high pressure area is offset to the side, located at the A column of the Car, but this position is not fixed in the platoon-driving.

4.2 Aerodynamic Force

There is a great difference in the absolute velocity of the airflow around the front and rear vehicles in the process of procession driving, so it is not suitable to use aerodynamic coefficient for comparative analysis, so the aerodynamic data is directly used in the following sections.

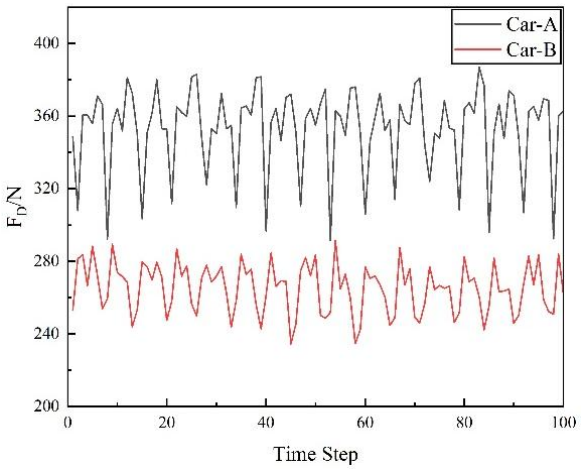

(a) Drag

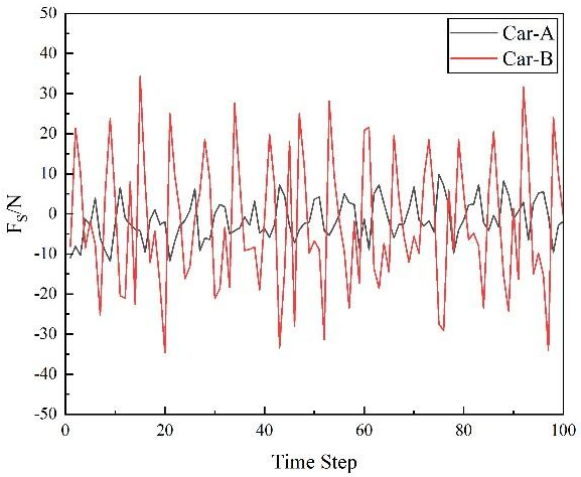

(b) Lateral force

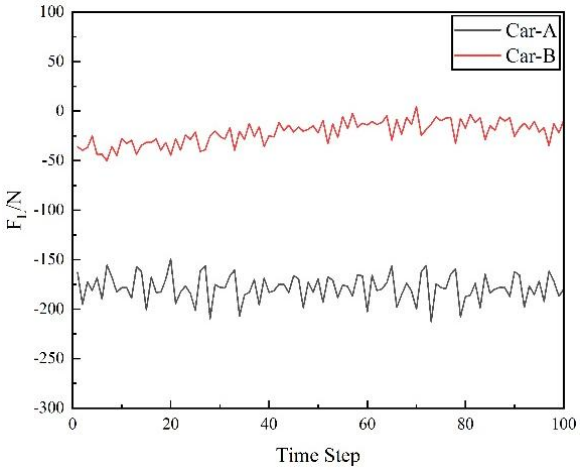

(c) Lift force

Figure 11. Aerodynamic force of platoon-driving

100 time steps were randomly intercepted from the monitored aerodynamic data for statistics, as shown in Figure 11. The drag of Car-B is significantly less than Car-A, whose average air resistance is 353.3N and that of Car-B is 265.3N, and the resistance of the two vehicles fluctuates back and forth in A small range during driving. In the platoon-driving, the mean lateral force of both vehicles is 0, but the lateral force fluctuation range of the rear Car-B is larger. Affected by the air flow flowing through the front car and the air vortex falling off the front car, the rear car is more significantly affected by the air disturbance, resulting in greater fluctuations on the side of the body. (Cui Weizheng, Qin Wenbin, Zhang Xiantang, Li Peng & Zhang Mingguang, 2018) The same reason will also cause the lift force of the car to change.

5. Influence of Car Meeting on Disturbance Transfer Characteristics of Platoon-Driving

In this paper, after sorting out the simulation results of the platoon-driving of car meeting condition, it is found that the drag and lift of vehicles have little changes, while the lateral force has an obvious peak. The driving behavior will affect the stability of vehicles to a certain extent, so this section focuses on the analysis of the lateral force and yaw moment of vehicles. In order to describe the position relationship of cars at different moments, the geometric center point of Car-C is m, and the center point of Car-A and Car-B is n, as shown in Figure 12. The distance between point m and point n along the X-axis is X, and X/L is used to describe the position relationship of cars.

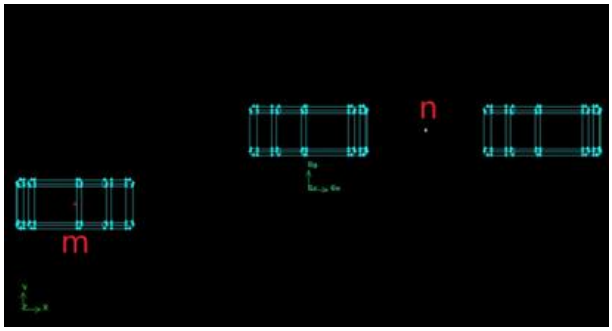

Figure 12. Schematic diagram of geometric center

5.1 Analysis of Lateral Force

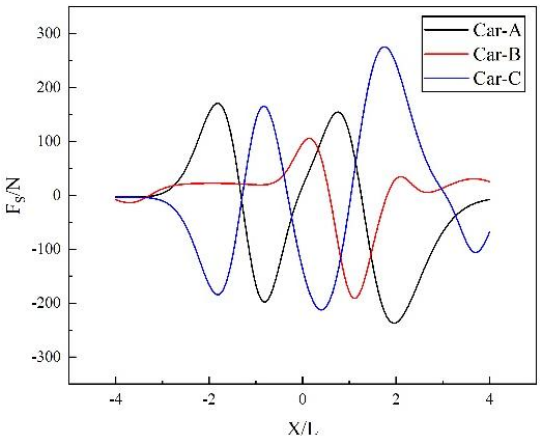

Figure 13. Fitting diagram of peak lateral force of each vehicle

Figure 13 shows the variation of lateral forces of vehicles at different positions. When X/L=-3, Car-A and Car-C are 1L away from each other in the X-axis direction, the lateral forces received by the two vehicles show mutual “repulsion”, and the value of lateral force rises sharply. The lateral force of Car-A reaches the maximum value of 200N, and then decreases sharply. At X/L=-1, a gap of 1L length is formed between Car-A and Car-C, and the lateral force of the two cars reaches another peak, at which time the two cars show a strong attraction tendency. Coincidentally, the distance between Car-B and Car-C is 1L. The lateral force of Car-B began to increase significantly. At X/L=0, the lateral force on Car-B reaches its peak, but the peak value is slightly smaller than

that of the front Car-A, which indicates that the “repulsion” force on the trailing Car is small at the beginning of the meeting, and the direction of the lateral force on CAR-C is opposite to that on Car-B. And it did not reach the peak at this time, but after continuing to drive a short distance, it reached the peak under the condition that the lateral force received by Car-B decreases. In addition, with the increase of the distance between Car-A and Car-C, there are certain fluctuations in the lateral force of Car-A, which is one of the reasons why the peak time of Car-C lateral force is delayed. When X/L=1, there is a long gap flow between Car-B and Car-C body, and the side force on Car-B reaches the second peak. There is a mutual “attraction” trend between Car-B and Car-C, and Car-C is affected by complex flow field, and its side force reaches the maximum at the position of X/L=1.5. This value is about 100N higher than the peak value of lateral force of cars in formation. After that, the lateral force of the three vehicles still has a small fluctuation, and the running state of the three vehicles gradually recovers to be stable when X/L=3.

5.2 Analysis of Yaw Moment

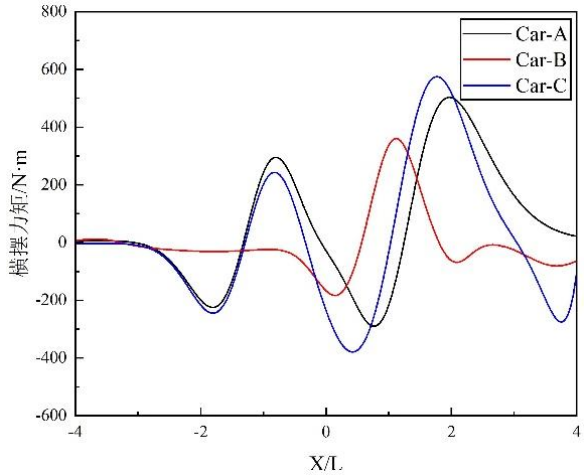

Figure 14. Peak yaw moment fitting diagram of each vehicle

Figure 14 shows the variation of the yaw moment of each vehicle. As a whole, the variation trend of the yaw moment of Car-A and Car-C is the same and the peak value is similar before X/L=-1. However, after X/L=-1, along with the enhanced interaction of air flow around the three vehicles, the variation of yaw moment of each vehicle showed great differences. Similar to the variation of lateral force, Car-B has the smallest variation of yaw moment, which indicates that the trailing vehicles in the lineup are less affected by the driving conditions and have better driving stability. Especially at X/L=0, Car-B and Car-C are flush at the front, and both cars produce clockwise yaw moment. However, the value of the yaw moment of Car-B is significantly smaller than that of Car-C, and the reason for this phenomenon is closely related to the driving state in the procession. In addition, Car-B’s yaw was the first to return to the normal driving state shortly after the race ended. This indicates that platoons have a great advantage in terms of stability in meeting conditions.

6. Conclusion

In this paper, the overlapping grid method is used to simulate the three working conditions of single vehicle driving, platoon-driving and platoon car meeting, and the following conclusions are drawn:

(1) By comparing the simulation results of single vehicle driving with the wind tunnel test data, it is found that the error is relatively small, which verifies the effectiveness of the overlapping grid method. Moreover, through the pressure cloud map, it is found that at the junction of the car geometry, the pressure decreases due to the effect of air separation, and there is negative pressure.

(2) In the process of procession, the air resistance of the rear car is significantly lower than that of the front car, which indicates that the small car model also has fuel economy benefits in procession; There is a certain difference in the surface pressure of the front and rear cars, and the position of the high-pressure area in the front face of the rear car is not fixed; The mean value of lateral force is 0, but the value fluctuation of the rear vehicle is more obvious.

(3) With the change of the position relation, the cars moving in the opposite direction will show the tendency of “repulsion” and “attraction” in the platoon car meeting condition. For the car in front, usually the “repulsive” force appears at the distance of 1 body, and reaches the maximum when the front is flush, and the “attractive”

force usually reaches the maximum when the head of one car is flush with the tail of another car. But for the rear car, affected by the airflow in front of the car, the peak position is slightly delayed, and the “repulsive” force is significantly weakened.

(4) The yaw moment of the trailing vehicles in the procession has the smallest variation when the procession is in the procession, and the yaw moment of the trailing vehicles in the procession first returns to the normal running state after the procession, which indicates that the procession cars have strong driving stability during the procession.

References

Charles-Henri Bruneau, Khodor Khadra, Iraj Mortazavi, (2017). Flow analysis of square-back simplified vehicles in platoon. *International Journal of Heat and Fluid Flow, 66*, pp.43-59.

Chen Jianhong, (2015). Numerical simulation of MIRA model outflow field based on CFD. *Journal of Heihe University, 6*(06), 117-119.

Cui Weizheng, Qin Wenbin, Zhang Xiantang, Li Peng, Zhang Mingguang, (2018). Study on influence factors of flow around twin tandem-circular cylinders under high Reynolds number. *Water Resources and Hydropower Engineering, 49*(2), 92-98.

Feng Yibin, Guo Xuexun, (2008). The application of FLUENT in automotive aerodynamics research. *Beijing Automotive Engineering*, (02), 38-42.

Francis H. Robertson, Frederick Bourriez, Mingzhe He, David Soper, Chris Baker, Hassan Hemida, Mark Sterling, (2019). An experimental investigation of the aerodynamic flows created by lorries travelling in a long platoon. *Journal of Wind Engineering and Industrial Aerodynamics, 193*, 103966.

Gao Long, Zhou Haichao, (2012). Research on Aerodynamic Characteristics During Speeding and Overtaking Processes in Tunnel. *Journal of Chongqing Jiaotong University (Natural Science)*, *31*(03), 465-468+472. (in Chinese)

Gu Zhengqi, Yang Binhui, Gong Xu, Sun Lu, Yuan Zhiqun, (2010). Analysis for Transient Aerodynamic Characteristics of Two Automobiles Passing Each Other. *Journal of Hunan University (Natural Science), 37*(06), 27-31.

Guanghan Peng, Shuhong Yang, Dongxue Xia, Xiaoqin Li, (2019). Delayed-feedback control in a car-following model with the combination of V2V communication, *Physica A: Statistical Mechanics and its Applications, 526*, 120912.

Jiang Tao, Shi Yan, Xu Peipei, Wang Min, Li Yao, (2022). Simulation of wind resistance and calculation of fuel saving rate of heavy truck formation driving. *Internal Combustion Engine and Power, 39*(03), 81-85.

Li Mingda, Wei Hailin, Men Yuzhuo, Bao Cuizhu, (2018). The Study on Aerodynamics Drag of Platooning Oil Tanker Trucks. *Journal of South China University of Technology (Natural Science Edition)*, *46*(04), 29-34+43.

Li Peng, Gao Zhenxun, Jiang Chongwen, (2014). The Progress of The Overlapping Grid Techniques. *Mechanics in Engineering, 36*(05), 551-565.

Tang Hongtao, Miao Xiuqi, Chen Guanghou, Dong Linyuan, (2018). Head Crossing Two-dimensional Aerodynamic Simulation for Automobiles. *Journal of Tianjin University of Science and Technology, 33*(04), 67-73. (in Chinese)

Wang Jingyu, Yu Xutao, Hui Zheng, Hu Xingjun, (2017). Influence of running speed and lateral distance on vehicle transient aerodynamic characteristics during curve crossing. *Journal of Jiangsu University (Natural Science Edition), 38*(03), 249-253+272.

Wang Shi, (2011). Experimental Investigation on Aerodynamic Characteristics of MIRA Model Group in Wind Tunnel. Hunan University.

Xiao-Tian Zhang, Francis H. Robertson, David Soper, Hassan Hemida, Shi-Di Huang, (2021). Investigation of the aerodynamic phenomena associated with a long lorry platoon running through a tunnel. *Journal of Wind Engineering and Industrial Aerodynamics, 210*, 104514.

Zhang Yingchao, Cao Huinan, Zhu Hui, (2019). Instantaneous Flow Structure Analysis of MIRA Notchback Model. *Journal of Hunan University (Natural Science), 46*(08), 51-58.

Zhang Yingchao, Li Jie, Li Yuhu, Hu Xingjun, Fu Limin, (2008). Numerical simulation of car aerodynamic characteristics when crossing each other. *Journal of Jiangsu University (Natural Science Edition)*, (02), 119-122.